

# Stability Analysis of the Immersed Boundary Method for a Two-dimensional Membrane with Bending Rigidity

Zhaoxin Gong<sup>1</sup>, Huaxiong Huang<sup>1,2</sup> and Chuanjing Lu<sup>1</sup>

**Abstract:** In this paper, we analyse the stability of the Immersed Boundary Method applied to a membrane-fluid system with a plasma membrane immersed in an incompressible viscous fluid. We show that for small deformations, the planar rest state is stable for a membrane with bending rigidity. The smoothed version, using a standard regularization technique for the singular force, is also shown to be stable. Furthermore, we show that the coupled fluid-membrane system is stiff and smoothing helps to reduce the stiffness. Compared to the system of elastic fibers immersed in an incompressible fluid, membrane with bending rigidity consist of a wider range of decay rates. Therefore numerical instability could occur more easily for an explicit method when the time step size is not sufficiently small, even though the continuous problem is stable.

**Keywords:** bending rigidity, immersed boundary method, membrane, moving interface, stability

## 1. Introduction

In nature as well as in engineering applications, there exist abundant examples where a flexible structure is immersed in a viscous incompressible fluid. Such a structure-fluid interaction is especially relevant in biological systems. The immersed boundary method, which was developed by Peskin [1] and Peskin and McQueen [2] to study the nature of the blood flow in the heart, is an effective technique for modeling and simulating this type of fluid-structure interactions. The immersed boundary method considers the structure as an immersed boundary, which can be represented by a singular force in the Navier-Stokes equations rather than a real body. It avoids difficulties associated with moving boundaries faced by conventional methods. The immersed boundary method is both a mathematical formulation and a numerical scheme. The mathematical formulation employs a mixture of Eulerian and Lagrangian variables. These are related by interaction equations in which the Dirac delta function plays a prominent role. The numerical implementation consists of

---

<sup>1</sup> Department of Mechanics, Shanghai Jiaotong University, Shanghai, 200240, China.

<sup>2</sup> Department of Mathematics and Statistics, York University, Toronto, Ontario, Canada M3J 1P3.

several steps. First of all, the Eulerian (field) variables are defined on a fixed Cartesian mesh while the Lagrangian variables (related to the immersed boundary) are defined on a curvilinear grid that lies on top of the fixed Cartesian mesh. Secondly, a smoothing (discretization) is needed for the Dirac delta function, constructed according to certain principles, e.g., by matching the moments. The immersed boundary method has been applied to a variety of problems, such as the swimming of eels, sperm and bacteria [3]~[5], ameboid deformation [6], platelet aggregation during blood clotting [7, 8], and the deformation of red blood cells in a shear flow [9].

Despite the popularity of the immersed boundary method as a computational tool, only few analyses have been given on the method itself. Beyer and LeVeque [10] provided one of the first convergence analyses using a one-dimensional model. Tu and Peskin [11] performed stability analysis for three different methods including the immersed boundary method for solving fluid flow problems with moving interfaces. Stockie [12] and Stockie and Wetton [13, 14] presented linear stability analysis on both continuous and discrete versions of the immersed boundary method applied to fluid flows with immersed fibers. All analyses above assumed that the immersed structure was elastic without bending resistance. On the other hand, biological cell membranes are nearly incompressible with bending rigidity. Thus bending resistance cannot be ignored in flow problems involving biological cells, especially when the curvature of the immersed boundary is large. Our aim in this paper is to analyse the stability of immersed boundary with bending resistance moving in an incompressible viscous fluid.

We consider a two-dimensional membrane immersed in a quiet flow field at the equilibrium state. We formulate the problem using the immersed boundary approach and carry out linear stability analysis by computing the eigenvalues of the membrane-fluid system in a periodic box. The smoothed version is considered next by regularizing the Dirac delta function, following Peskin [1]. Without regularization (smoothing), the singular delta function leads to jumps in the pressure and the velocity gradient. One can use these jump conditions to construct numerical method, such as the immersed interface method proposed by LeVeque and Li [15] and analysed by

Huang and Li [16]. Therefore, the analysis of the unsmoothed version is more relevant to the immersed interface method while that of the smoothed version is directly related to the immersed boundary method used in [1]~[9]. Our analysis shows that both versions are linearly stable but the membrane with bending rigidity is more stiff than the (linear) elastic membrane-fluid system. Thus, the system with bending resistive membrane is more difficult to solve from computational point of view.

## 2. Mathematical Model

For flow problems with immersed flexible structure, there are two distinct approaches. The first approach, or moving grid methods, treats the immersed boundary as a boundary and applies the jump conditions directly. The solution domain is divided by the immersed boundary and coupled together by the jump conditions. The flow equations are solved using moving finite volume or finite element methods [17, 18]. The second approach, or fixed grid methods, follows the immersed boundary implicitly, either by capturing or tracking. The capturing methods include the well-known level-set and phase-field methods where the immersed boundary (interface) coincides with a level curve (surface) of an auxiliary variable or an order parameter, which is convected by the flow field [19, 20]. The immersed boundary method is a tracking scheme where the immersed boundary is represented by a singular forcing term and tracked in a Lagrangian fashion while the fields variables are defined and solved on a fixed grid in an Eulerian setting. To solve flow problems using the immersed boundary method, the singular forcing term needs to be regularized. Here we distinguish the original and regularized versions of the immersed boundary method as the “sharp interface problem” and “smoothed problem”, respectively.

We assume that the fluid is incompressible with constant viscous and constant density. For biological applications at the cellular level, the Reynolds number is typically small. Therefore, we can use Stokes approximation instead of the Navier-Stokes equations as the governing equations. We start by setting up the sharp

interface problem first.

## 2.1 Sharp interface problem

The size of the red blood cells and other relevant biological cells are typically small (in the micrometer range). Therefore, the fluid inertia is small compared with the viscous force, i.e., the Reynolds number of the flow is small. On the other hand, the presence of the immersed boundary introduces an intrinsic time scale related to deformation of the membrane and the unsteadiness parameter is of order one, cf. Pozrikidis [21]. Therefore, the motion of the fluid field is governed by unsteady Stokes equations

$$\rho \frac{\partial \mathbf{u}}{\partial t} = -\nabla p + \mu \Delta \mathbf{u}, \quad (1)$$

$$\nabla \cdot \mathbf{u} = 0, \quad (2)$$

where  $\rho$  is the fluid density,  $\mu$  is the fluid viscosity,  $\mathbf{u}(\mathbf{x}, t)$  and  $p(\mathbf{x}, t)$  are the fluid velocity and pressure. The jump conditions for immersed material are

$$[\mathbf{u}] = \mathbf{0}, \quad (3)$$

$$\mu \left[ \frac{\partial \mathbf{u}}{\partial y} \right] = - \frac{\mathbf{f} \cdot \boldsymbol{\tau}}{|\partial \mathbf{X} / \partial s|} \boldsymbol{\tau}, \quad (4)$$

$$[p] = \frac{\mathbf{f} \cdot \mathbf{n}}{|\partial \mathbf{X} / \partial s|}, \quad (5)$$

where  $[\cdot] = (\cdot)|_{\Omega^+} - (\cdot)|_{\Omega^-}$  denotes the jump across the interface,  $\mathbf{f}(s, t)$  is the force density along the immersed boundary,  $\mathbf{X}(s, t)$  denotes the immersed boundary position prescribed by the kinematic condition (carrying by the fluid velocity),  $s$  is the arclength along the membrane,  $\mathbf{n}$  is the unit normal vector,  $\boldsymbol{\tau}$  is the unit tangent to the immersed boundary.

## 2.2 Smoothed problem

The governing equations are Stokes equations

$$\rho \frac{\partial \mathbf{u}}{\partial t} = -\nabla p + \mu \Delta \mathbf{u} + \mathbf{F}, \quad (6)$$

$$\nabla \cdot \mathbf{u} = 0, \quad (7)$$

where  $\mathbf{F}(\mathbf{x}, t)$  is the fluid body force. Since the immersed boundary is constrained to

move at the same velocity as neighboring fluid particles, the interaction equation for velocity can be written as:

$$\frac{\partial \mathbf{X}}{\partial t}(s, t) = \mathbf{u}(\mathbf{X}(s, t), t) = \int \mathbf{u}(\mathbf{x}, t) \delta(\mathbf{x} - \mathbf{X}(s, t)) d\mathbf{x}, \quad (8)$$

and  $\mathbf{F}(\mathbf{x}, t)$  can be expressed as :

$$\mathbf{F}(\mathbf{x}, t) = \int \mathbf{f}(s, t) \delta(\mathbf{x} - \mathbf{X}(s, t)) ds, \quad (9)$$

where  $\delta$  denotes the three dimensional Dirac delta function. It can be shown that the system of equations (6)~(9) is equivalent to (1)~(5) [22]. To solve it numerically, (6) and (7) are discretized on a fixed Eulerian grid while (8) is approximated by markers on the membrane and tracked explicitly. Finally, the Dirac delta function in (8) and (9) can be regularized in different ways, as long as certain moment and other conditions are satisfied, cf. [22]. In this paper, we use the original function proposed in [1] and it can be written as follows:

$$\delta_h(\mathbf{x}) = \frac{1}{h^2} \phi\left(\frac{x_1}{h}\right) \phi\left(\frac{x_2}{h}\right), \quad (10)$$

$$\phi(r) = \begin{cases} \frac{1}{4} \left(1 + \cos\left(\frac{\pi r}{2}\right)\right), & |r| \leq 2, \\ 0, & |r| > 2, \end{cases} \quad (11)$$

where  $x_1$  and  $x_2$  are the Cartesian component of  $\mathbf{x}$  and  $h$  is the grid size.

### 3. Linear Stability Analysis

In [14], Stockie analysed the immersed boundary method by examining a fluid-fiber system where elastic fibers are immersed in an incompressible viscous fluid. It was showed that such system was linearly stable but stiff. Our objective is to extend Stockie's work and analyse the stability of a fluid-membrane system where bending resistance is the dominant force. To simplify the analysis, a 2-D fluid field with an immersed membrane inside a periodic box is considered in this paper.

Let  $\Gamma$  denote the immersed membrane in fluid domain  $\Omega$ , which divides the

whole domain into two sub-domains  $\Omega^+$  and  $\Omega^-$ . We consider a portion of the fluid domain in which the immersed membrane is approximately flat, labeled as  $\Omega_0$ . In order to isolate the influence of the membrane on the flow, the boundaries of  $\Omega_0$  are extended to infinity in the  $y$ -direction and periodically in the other direction (Fig. 1).

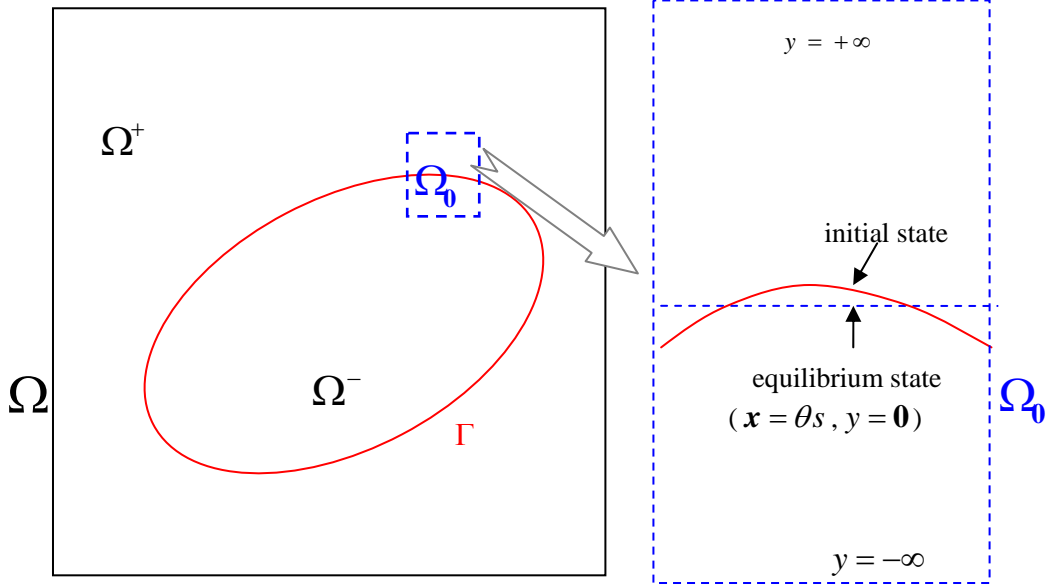


Figure 1: 2-D fluid domain containing immersed membrane.

Suppose the equilibrium state of the membrane in  $\Omega_0$  defined by  $y=0$  and  $\mathbf{x} = \theta s$ , where  $s$  is the corresponding un-deformed arc-length and  $\theta = |\partial \mathbf{X} / \partial s| \geq 1$ . In such position, the force acting on the fiber could be zero. Assume that the membrane is hyper-elastic and with bending rigidity, its force density can be expressed as

$$\mathbf{f}(l, t) = \frac{\partial}{\partial l} (T \boldsymbol{\tau} + q \mathbf{n}) = \left( \kappa T + \frac{\partial q}{\partial l} \right) \mathbf{n} + \left( \frac{\partial T}{\partial l} - \kappa q \right) \boldsymbol{\tau}, \quad (12)$$

where  $T$  is in-plane tension,  $q = \partial M / \partial l$  is the transverse shear tension,  $M$  is the bending moment,  $l$  is the arc-length,  $\kappa$  is the curvature satisfying  $\partial \boldsymbol{\tau} / \partial l = \kappa \mathbf{n}$ ,  $\partial \mathbf{n} / \partial l = -\kappa \boldsymbol{\tau}$ . In this paper we use the Evans & Skalak (ES) law [23, 24] for the in-plane tension

$$T = C_{ES} \left( \frac{1}{(ds/dl)^2} - (ds/dl)^2 \right), \quad (13)$$

and a linear relation for the bending moment

$$M = E_B (\kappa - \kappa_0), \quad (14)$$

where  $C_{ES}$  is the ratio of the surface shear modulus to the Young modulus,  $E_B$  is the bending modulus and  $\kappa_0$  is the curvature at equilibrium. Since  $s$  is the corresponding un-deformed arc-length,  $ds/dl = 1/|\partial\mathbf{X}/\partial s|$ . The local force density per unit length  $\mathbf{f}(s, t)$  is given by

$$\mathbf{f}(s, t) = \mathbf{f}(l, t) |\partial\mathbf{X}/\partial s|, \quad (15)$$

Denote  $(\xi, \eta)$  as a perturbation to the membrane position, and assume  $\xi, \eta, \mathbf{u}$  and their derivatives are small, the membrane position  $\mathbf{X}(s, t)$  takes the form

$$\mathbf{X}(s, t) = (\theta s + \xi(s, t), \eta(s, t)), \quad (16)$$

Differentiating (16) with respect to  $s$  and dropping the (higher order) nonlinear terms yields

$$\frac{\partial\mathbf{X}}{\partial s} \approx \left( \theta + \frac{\partial\xi}{\partial s}, \frac{\partial\eta}{\partial s} \right), \quad (17)$$

$$\begin{aligned} \left| \frac{\partial\mathbf{X}}{\partial s} \right| &\approx \sqrt{\left( \theta + \frac{\partial\xi}{\partial s} \right)^2 + \left( \frac{\partial\eta}{\partial s} \right)^2}, \\ &\approx \theta + \frac{\partial\xi}{\partial s}, \end{aligned} \quad (18)$$

Expanding (13) in a Taylor series about the equilibrium state  $|\partial\mathbf{X}/\partial s| = \theta$ , we obtain

$$T \approx C_{ES} \left( \theta^2 - \frac{1}{\theta^2} \right) + 2C_{ES} \left( \theta + \frac{1}{\theta^3} \right) \frac{\partial\xi}{\partial s}, \quad (19)$$

Combining (19) and the linearized expression for curvature  $\kappa$ ,

$$\kappa = \frac{\partial^2 |\mathbf{X}|}{\partial s^2} \approx \frac{1}{\theta^2} \frac{\partial^2 \eta}{\partial s^2}, \quad (20)$$

the force density in the normal and tangential directions can be expressed as follows:

$$\begin{aligned} f_n(l,t) &= \kappa T + \frac{\partial q}{\partial l}, \\ &\approx \sigma_n \frac{\partial^2 \eta}{\partial s^2} + \phi_n \frac{\partial^4 \eta}{\partial s^4}, \end{aligned} \quad (21)$$

$$\begin{aligned} f_\tau(l,t) &= \frac{\partial T}{\partial l} - \kappa q, \\ &\approx \sigma_\tau \frac{\partial^2 \xi}{\partial s^2}, \end{aligned} \quad (22)$$

where  $\phi_n = E_B/\theta^4 \geq 0$ ,  $\sigma_n = C_{ES}(1-1/\theta^4) \geq 0$ , and  $\sigma_\tau = 2C_{ES}(1+1/\theta^4) \geq 0$ . For small perturbations from the equilibrium state, above formulae show that bending moment acts mainly in the normal direction and its role in tangential direction can be ignored. We now discuss the stability of the membrane-fluid system using the sharp interface formulation and its smoothed version.

### 3.1 Linear stability of the sharp interface problem

In our problem, the jump conditions (3)~(5) can be written as [13]

$$[\mathbf{u}] = \mathbf{0}, \quad (23)$$

$$\mu \left[ \frac{\partial \mathbf{u}}{\partial y} \right] = - \frac{\mathbf{f} \cdot \boldsymbol{\tau}}{|\partial \mathbf{X} / \partial s|} \boldsymbol{\tau}, \quad (24)$$

$$[p] = \frac{\mathbf{f} \cdot \mathbf{n}}{|\partial \mathbf{X} / \partial s|}, \quad (25)$$

Rewrite the unknowns in the sub-domain  $\Omega_0^+$  and  $\Omega_0^-$  in the form of Fourier modes

$$\begin{Bmatrix} u \\ v \\ p \end{Bmatrix}^\pm = e^{\lambda t + i\alpha x} \begin{Bmatrix} \hat{u}(y) \\ \hat{v}(y) \\ \hat{p}(y) \end{Bmatrix}^\pm, \quad \begin{Bmatrix} \xi \\ \eta \end{Bmatrix}^\pm = e^{\lambda t + i\alpha s} \begin{Bmatrix} \hat{\xi} \\ \hat{\eta} \end{Bmatrix}^\pm, \quad (26)$$

where,  $\alpha > 0$  is the wave number,  $i = \sqrt{-1}$  is the imaginary unit,  $\lambda$  embodies the decay (or growth) characteristics of each solution mode. Substitute (26) into the Stokes equations (1) and (2), and introduce the following parameters:  $\hat{\mathbf{u}}^* = \frac{\hat{\mathbf{u}}}{U}$ ,

$\hat{p}^* = \frac{\hat{p}}{(\phi_n/L^3 + \sigma_n/L)}$ ,  $y^* = \frac{y}{L}$ ,  $\alpha^* = \frac{\alpha}{1/L}$ ,  $\lambda^* = \frac{\lambda}{\mu/(\rho L^2)}$ , then the governing

equations can be written as:

$$\frac{1}{Re} \left( \lambda^* - \frac{d^2}{dy^{*2}} + \alpha^{*2} \right) \widehat{u}^* = -Er (i\alpha^* \widehat{p}^*), \quad (27)$$

$$\frac{1}{Re} \left( \lambda^* - \frac{d^2}{dy^{*2}} + \alpha^{*2} \right) \widehat{v}^* = -Er \left( \frac{d\widehat{p}^*}{dy^*} \right), \quad (28)$$

$$i\alpha^* \widehat{u}^* + \frac{d\widehat{v}^*}{dy^*} = 0, \quad (29)$$

where  $Re = \frac{\rho UL}{\mu}$  is the Reynolds number and  $Er = \frac{\phi_n + \sigma_n L^2}{\rho U^2 L^3}$  is the ratio between the bending moment and the inertia force. Using MAPLE to solve the eigenvalue problem (27)~(29) and imposing the requirement that  $\widehat{u}^*, \widehat{v}^*, \widehat{p}^*$  are bounded as  $y^* \rightarrow \pm\infty$ , we obtain the following expressions

$$\widehat{p}^{*(\pm)}(y^*) = \pm A^\pm \frac{\lambda^*}{Re \cdot Er \cdot \alpha^*} e^{\mp \alpha^* y^*}, \quad (30)$$

$$\widehat{u}^{*(\pm)}(y^*) = \mp i \left( A^\pm e^{\mp \alpha^* y^*} + \frac{\beta^*}{\alpha^*} B^\pm e^{\mp \beta^* y^*} \right), \quad (31)$$

$$\widehat{v}^{*(\pm)}(y^*) = A^\pm e^{\mp \alpha^* y^*} + B^\pm e^{\mp \beta^* y^*}, \quad (32)$$

where the new parameter  $\beta^*$  satisfies

$$\beta^{*2} = \alpha^{*2} + \lambda^*. \quad (33)$$

Without the loss of generality we assume that  $\text{Re}(\beta^*) \geq 0$  and  $\beta^* \neq \alpha^*$ , then  $\widehat{\xi}^*$  and  $\widehat{\eta}^*$  can be obtained by substituting (31) and (32) into the expressions for the membrane position

$$\widehat{\xi}^* = -\frac{i}{\lambda^*} (A^+ + \frac{\beta^*}{\alpha^*} B^+) \cdot Re, \quad (34)$$

$$\widehat{\eta}^* = (A^+ + B^+) \cdot Re / \lambda^*, \quad (35)$$

Provided that the coefficients  $A^\pm$  and  $B^\pm$  can be determined and the viscosity is continuous across the membrane. Substituting (34) and (35) into the jump conditions (23)~(25) we obtain:

$$[u^*] = 0, \quad (36)$$

$$[v^*] = 0, \quad (37)$$

$$\left[ \frac{\partial u^*}{\partial y^*} \right] = -Re \cdot Er \cdot \omega_\tau \cdot \alpha^{*2} \hat{\xi}^*, \quad (38)$$

$$[p^*] = \omega_n \alpha^{*2} \hat{\eta}^* + (1 - \omega_n) \alpha^{*4} \hat{\eta}^*, \quad (39)$$

where  $\omega_\tau = \sigma_\tau L^2 / (\phi_n + \sigma_n L^2)$  is the tangential elastic tension weight coefficient and  $\omega_n = \sigma_n L^2 / (\phi_n + \sigma_n L^2)$  is the normal elastic tension weight coefficient. Combining (30)~(32) with (36)~(39) leads to a homogeneous system with four unknowns coefficients:

$$\begin{bmatrix} -i & -i & -i\beta^*/\alpha^* & -i\beta^*/\alpha^* \\ -1 & 1 & -1 & 1 \\ -i\alpha^*\lambda^* & i\alpha^*(\lambda^* + Re^2 \cdot Er \cdot \omega_\tau \alpha^*) & -i\beta^{*2} \lambda^*/\alpha^* & i\beta^* \left( \frac{\beta^* \lambda^{*2}}{\alpha^*} + Re^2 \cdot Er \cdot \omega_\tau \alpha^* \right) \\ \frac{\lambda^{*2}}{\alpha^*} & \frac{\lambda^{*2}}{\alpha^*} + Re^2 \cdot Er((1 - \omega_n)\alpha^{*4} + \omega_n \alpha^{*2}) & 0 & -Re^2 \cdot Er((1 - \omega_n)\alpha^{*4} + \omega_n \alpha^{*2}) \end{bmatrix} \cdot \begin{bmatrix} A^- \\ A^+ \\ B^- \\ B^+ \end{bmatrix} = \begin{bmatrix} 0 \\ 0 \\ 0 \\ 0 \end{bmatrix} \quad (40)$$

In order to obtain a non-trivial solution of (40), the determinant of the coefficient matrix must be zero. After some algebraic manipulations, the following expression can be obtained

$$\begin{aligned} & (\beta^{*4} + \alpha^* \beta^{*3} - \alpha^{*2} \beta^{*2} - \alpha^{*3} \beta^* + Re^2 \cdot Er \cdot (\omega_n \cdot \alpha^{*3} + (1 - \omega_n) \cdot \alpha^{*5}) / 2) \cdot \\ & (\beta^{*3} + \alpha^* \beta^{*2} - \alpha^{*2} \beta^* - \alpha^{*3} + Re^2 \cdot Er \cdot \omega_\tau \cdot \alpha^{*2}) = 0 \end{aligned} \quad (41)$$

This is a dispersion relation for the coupled membrane-fluid system. In [14], a similar equation was obtained and analysed for a two-dimensional elastic fiber immersed in an incompressible viscous fluid. In fact, the second factor in (41), which gives the solution related only to the shear membrane tension, is exactly the same. The eigenvalues associated to the in-plane tension and the bending rigidity are given by the first factor in (41). It can be seen clearly that the bending rigidity become more dominant for high frequency modes while the in-plane tension is more important for low frequency modes. In this paper, we focus our discussion related to the bending

resistance. Let  $\omega_n = \omega_\tau = 0$ , namely, neglect the tension effect, then the dispersion relation becomes

$$\left(\beta^{*4} + \alpha^* \beta^{*3} - \alpha^{*2} \beta^{*2} - \alpha^{*3} \beta^* + Re^2 \cdot Er \cdot \alpha^{*5}/2\right) \cdot \left(\beta^{*3} + \alpha^* \beta^{*2} - \alpha^{*2} \beta^* - \alpha^{*3}\right) = 0. \quad (42)$$

Before discussing the detailed numerical results, some interesting observations can be made. The second factor in (42), in the absence of in-plane tension, does not have any admissible roots. Thus we only need to find the zeros using the first factor of (42). Once  $\beta^*$  is obtained, the value of the growth/decay parameter  $\lambda^*$  can be computed from  $\lambda^* = \beta^{*2} - \alpha^{*2}$ . The growth or decay rate of solution is given by the real part of  $\lambda^*$  while the imaginary part of  $\lambda^*$  governs the oscillatory behavior of the modes. If  $\text{Re}(\lambda^*) \leq 0$  for all membrane modes, the modes decay in time and are stable; otherwise, solutions are unstable.

In order to simplify the dispersion relation more, we introduce three parameters

$$\left. \begin{aligned} \tilde{\alpha} &= \alpha^* \cdot (Re^2 \cdot Er), \\ \tilde{\beta} &= \beta^* \cdot (Re^2 \cdot Er), \\ \tilde{\lambda} &= \lambda^* \cdot (Re^2 \cdot Er)^2. \end{aligned} \right\} \quad (43)$$

For tensionless membrane, the non-dimension form of the dispersion relation can be expressed as

$$\tilde{\beta}^4 + \tilde{\alpha} \tilde{\beta}^3 - \tilde{\alpha}^2 \tilde{\beta}^2 - \tilde{\alpha}^3 \tilde{\beta} + \tilde{\alpha}^5/2 = 0 \quad (44)$$

with  $\tilde{\lambda} = \tilde{\beta}^2 - \tilde{\alpha}^2$ . Two admissible roots of  $\tilde{\beta}$  ( $\text{Re}(\tilde{\beta}) \geq 0$ ) can be obtained by solving (44), and the values for  $\text{Re}(\tilde{\lambda})$  can be obtained correspondingly.

As seen in Fig. 2, the real part of  $\tilde{\lambda}$  is non-positive, i.e.  $\text{Re}(\tilde{\lambda}) \leq 0$ , which means all membrane modes are stable. In fact, the stability of all membrane modes under bending resistance can be shown rigorously as follows. Let  $\tilde{\beta} = \tilde{\alpha} z^*$ ,  $z^* = x^* + iy^* \in \mathbb{C}$  and denote the relevant factor in (44) as

$$f(z^*) = z^{*4} + z^{*3} - z^{*2} - z^* + \tilde{\alpha}/2, \quad (45)$$

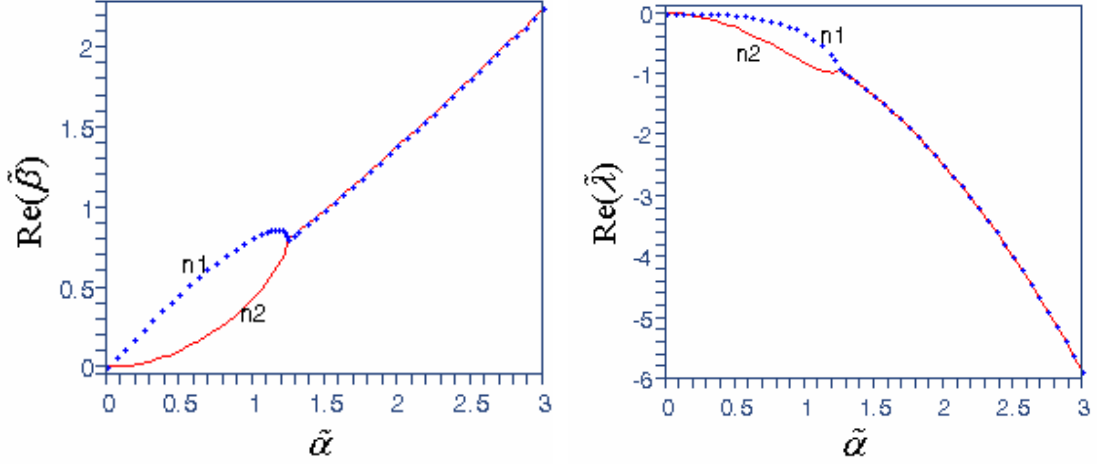


Figure 2: Plots of  $\text{Re}(\tilde{\beta})$  and  $\text{Re}(\tilde{\lambda})$  versus  $\tilde{\alpha}$  for sharp interface problem.

where  $x^* = \text{Re}(z^*) > 0$  and  $\text{Re}(\tilde{\lambda}) = x^{*2} - y^{*2} - 1$ . If  $x^{*2} \geq y^{*2} + 1$  and  $y^* > 0$ , then

$$\begin{aligned}
 \text{Im}(f) &= y^* (4x^{*3} + 3x^{*2} - 2x^* - 1 - y^{*2}(4x^* + 1)), \\
 &\geq y^* (4x^{*3} + 3x^{*2} - 2x^* - 1 + (1 - x^{*2})(4x^* + 1)), \\
 &= 2x^* y^* (x^* + 1) > 0,
 \end{aligned} \tag{46}$$

which contradicts the fact that any root of  $f(z)$  must satisfy  $\text{Re}(f) = \text{Im}(f) = 0$ . Therefore,  $x^{*2} < y^{*2} + 1$  for all roots when  $y^* > 0$ . Similarly, the same results can be obtained when  $y^* = 0$  and  $y^* < 0$ . It shows that  $\text{Re}(\tilde{\lambda}) < 0$  for  $\tilde{\beta} \in \mathbb{C}$ , i.e. all membrane modes are stable.

We now turn our attention to the smoothed problem and discuss the effect of the regularization on the linear stability of the membrane-fluid system using the immersed boundary method.

### 3.2 Linear stability of the smoothed problem

For the purpose of investigating the smoothed problem, domain  $\Omega_0$  is divided by interfaces  $y = \pm \varepsilon$ , where  $\varepsilon$  is the regularization parameter representing the radius of support of the approximate delta function. Therefore, in domain  $\Omega_0$ , there are three sub-domains: upper domain  $\Omega_0^+$ , smoothing domain  $\Omega_0^\varepsilon$  and lower domain  $\Omega_0^-$ , as shown in Fig.3. Non-dimensionalize all variables using the same parameters as in sharp interface problem. In sub-domains  $\Omega_0^+$  and  $\Omega_0^-$ , the influence of the

membrane is neglected, so the solutions on these two domains are identical with solutions of the sharp interface problem (30)~(32).

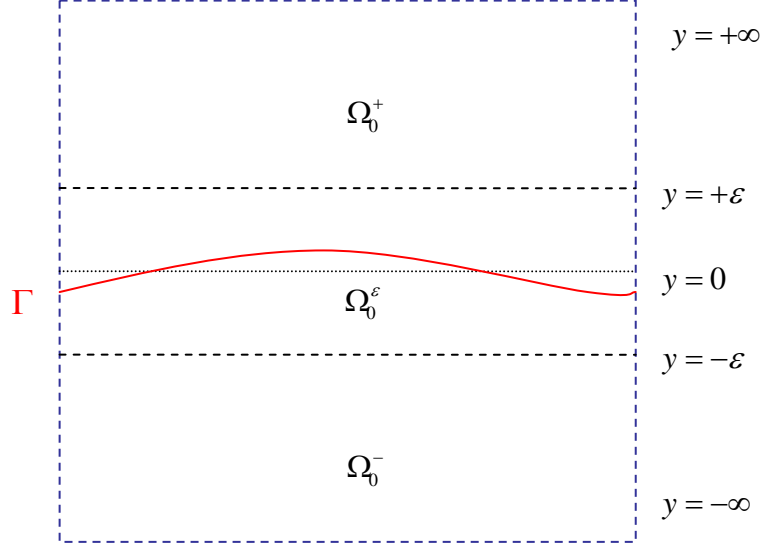


Figure 3: Repartition of domain  $\Omega_0$  into  $\Omega_0^+$ ,  $\Omega_0^\varepsilon$  and  $\Omega_0^-$ .

In the smoothing region  $\Omega_0^\varepsilon$ , the membrane has an effect on the fluid field. In order to obtain the solution in this domain, the smoothed Dirac delta function is introduced

$$\delta_\varepsilon(x) = \begin{cases} \frac{1}{2\varepsilon} \left( 1 + \cos\left(\frac{\pi x}{\varepsilon}\right) \right), & |x| < \varepsilon, \\ 0, & |x| \geq \varepsilon, \end{cases} \quad (47)$$

Let  $\widehat{D}_\alpha^\varepsilon = \int_{-\varepsilon}^{\varepsilon} e^{\pm i\alpha r} \delta_\varepsilon(r) dr$  and substitute (47) into it, we have

$$\widehat{D}_\alpha^\varepsilon = \frac{\pi^2 \sin(\alpha\varepsilon)}{\alpha\varepsilon(\pi^2 - \alpha^2\varepsilon^2)}, \quad (48)$$

Express the unknowns in the smoothing region in the form of Fourier modes, similar to the ones in equation (26), substitute the Fourier modes with (47) and (48) into the dimensionless form of (6)~(9), the governing equations in  $\Omega_0^\varepsilon$  become:

$$\frac{1}{Re} \left( \lambda^* - \frac{d^2}{dy^{*2}} + \alpha^{*2} \right) \widehat{u}^{*\varepsilon} = -Er \left( i\alpha^* \widehat{p}^{*\varepsilon} + \omega_i \theta \alpha^{*2} D^* \widehat{\xi}^* \delta_h(y^*) \right), \quad (49)$$

$$\frac{1}{Re} \left( \lambda^* - \frac{d^2}{dy^{*2}} + \alpha^{*2} \right) \widehat{v}^{*\varepsilon} = -Er \left( \frac{d\widehat{p}^{*\varepsilon}}{dy^*} + (\omega_n + (1-\omega_n)\alpha^{*2}) \theta \alpha^{*2} D^* \widehat{\eta}^* \delta_h(y^*) \right), \quad (50)$$

$$i\alpha^* \widehat{u}^{*\varepsilon} + \frac{d\widehat{v}^{*\varepsilon}}{dy^*} = 0. \quad (51)$$

And  $\widehat{\xi}^*$  and  $\widehat{\eta}^*$  can be obtained using the expressions membrane position

$$\lambda^* \widehat{\xi}^* = Re \cdot \widehat{D}^* \int_{-\varepsilon}^{\varepsilon} \widehat{u}^{*\varepsilon}(y^*) \delta_h(y^*) dy^*, \quad (52)$$

$$\lambda^* \widehat{\eta}^* = Re \cdot \widehat{D}^* \int_{-\varepsilon}^{\varepsilon} \widehat{v}^{*\varepsilon}(y^*) \delta_h(y^*) dy^*, \quad (53)$$

where

$$\widehat{D}^* = \frac{\pi^2 \sin(\alpha^* \varepsilon)}{\alpha^* \varepsilon (\pi^2 - \alpha^{*2} \varepsilon^2)}. \quad (54)$$

Equations (49)~(54) for the smoothing domain  $\Omega_0^\varepsilon$  are coupled with (30)~(32) for the outer regions. The expressions for  $\widehat{u}^{*\varepsilon}, \widehat{v}^{*\varepsilon}, \widehat{p}^{*\varepsilon}$  consist four coefficients  $D^\pm$  and  $C^\pm$ , plus four coefficients  $A^\pm$  and  $B^\pm$  form the expressions for  $\widehat{u}^*, \widehat{v}^*, \widehat{p}^*$  in domains  $\Omega_0^+$  and  $\Omega_0^-$ , as in equations (30)~(32). There are eight coefficients in all for the entire domain of the fluid field. Since pressure and velocity are continuous at the interface  $y^* = \pm\varepsilon$  and  $\widehat{u}^*, \widehat{v}^*, \widehat{p}^*$  are bounded as  $y^* \rightarrow \pm\infty$ , a system of eight homogeneous linear equations for eight unknown coefficients can be obtained. The dispersion relation can be derived in the same way outlined earlier. However, the expression is length and symbolically it can be written as

$$S_\tau(\beta^*) \cdot S_n(\beta^*) = 0, \quad (55)$$

where  $S_\tau(\beta^*)$  does not contain the normal force effects and  $S_n(\beta^*)$  does not contain the tangential force effects, except that both of them consist of a combination of polynomials and transcendental (trigonometric and exponential) functions of  $\beta^*$ . The dimensionless parameters  $Re$  and  $Er$  only appear in the group of  $(Re^2 \cdot Er)$ . Again, we only consider the bending resistance and take  $\omega_\tau = \omega_n = 0$ . Due to the complex nature of (55), we are not able to obtain analytical expression for  $\beta^*$ . Therefore, stability for the smoothed problem is investigated numerically. We note that the same problem occurred for elastic fibers and the eigenvalues are also solved

numerically in [12].

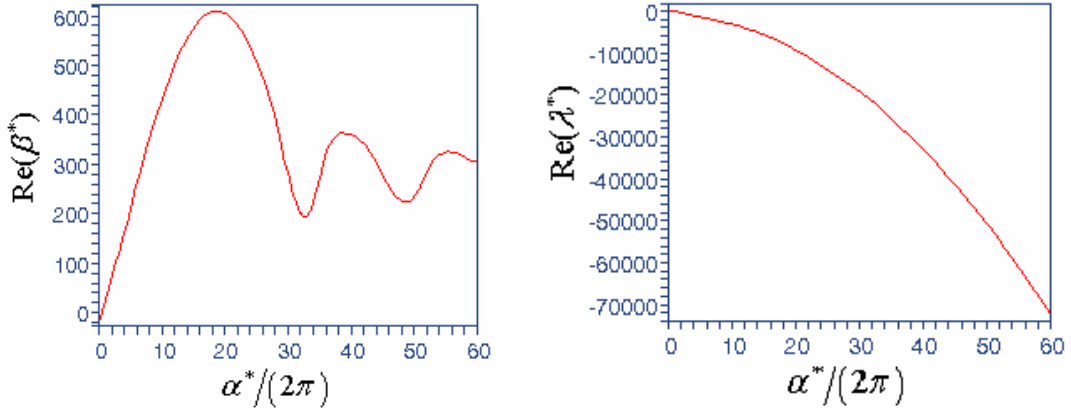


Figure 4: Plots of  $\text{Re}(\beta^*)$  and  $\text{Re}(\lambda^*)$  versus  $\alpha^*$  with  $Re=1, Er=10^3$  and  $\varepsilon=2/64$ .

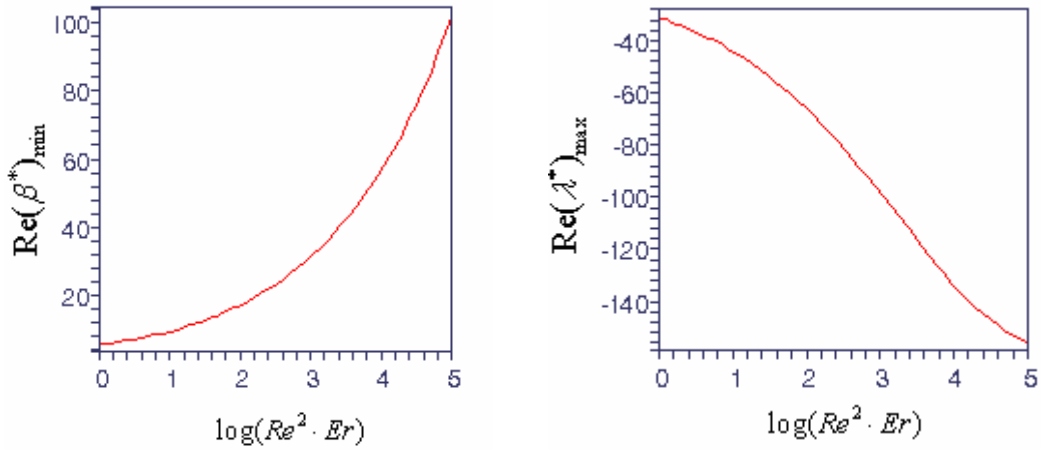


Figure 5: Plots of  $\text{Re}(\beta^*)_{\min}$  and  $\text{Re}(\lambda^*)_{\max}$  versus  $\log(Re^2 \cdot Er)$  with  $\varepsilon=2/64$ .

Consider a unit square computational region covered by an equally spaced grid with grid space  $h=1/N$  and radius of support of the approximate delta function  $\varepsilon=2/N$ . For a discrete set of wave-numbers  $\alpha^*=2\pi \cdot i$ ,  $i=\{1,2,3 \dots N\}$ , we compute the zeros of equation (55) by taking a representative parameter set  $Re=1$ ,  $Er=10^3$ . Because of the transcendental functions in equation (55), it is not clear how many roots exist. We first use MAPLE to solve (55), which yields one pair of conjugate roots with  $\text{Re}(\beta^*) \geq 0$  for each value of  $\alpha^*$ . We partition the complex

domain and no additional roots are found. We have also used MATLAB and find the same roots with at least 6 significant digits. Therefore, numerical evidences suggest that this pair is the only admissible roots, which corresponding to the smallest value of  $|\text{Re}(\lambda^*)|$ . Since the smooth version of the immersed boundary method is an approximation of the original sharp interface formulation, where only one pair of admissible roots exists, it is not surprising that the situation is similar. In Fig. 4, the plots of  $\text{Re}(\beta^*)$  and  $\text{Re}(\lambda^*)$  are given. It can be observed that the admissible solution satisfies  $\text{Re}(\beta^*) \geq 0$  and  $\text{Re}(\lambda^*) \leq 0$  for all  $\alpha^*$ . Furthermore, it can be seen from Fig. 4 that  $\text{Re}(\beta^*)$  reaches its minimum value at critical  $\alpha^*$  values ( $\alpha^* = 2\pi$ ) and the corresponding value of  $\lambda^*$  reach its maximum value of  $\text{Re}(\lambda^*)$ . In Fig. 5, we plot this minimum value of  $\text{Re}(\beta^*)$  and the corresponding maximum value of  $\text{Re}(\lambda^*)$  against with the assembled parameter ( $Re^2 \cdot Er$ ). It can be seen that the values of corresponding  $\text{Re}(\lambda^*)$  are always negative. Thus the bending resistive membrane-fluid system is stable using the immersed boundary method.

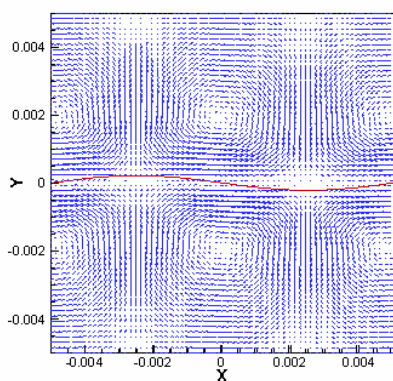
Combining our results and those in [14], it can be concluded here that the immersed membrane is linearly stable under elastic tension as well as bending rigidity. This conclusion is not a surprise because both elastic force and bending moment can be regarded as restoring forces, which makes the membrane go back to its equilibrium state when it is perturbed.

### 3.3 Numerical experiments

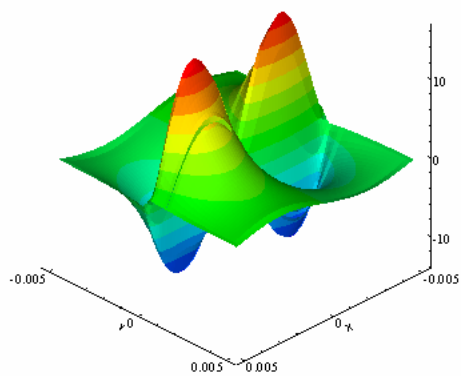
We assume that the fiber is only under the restoring bending force, which satisfies linear relation given in equation (15) and take an  $L \times L$  square as the computational domain, where  $L$  is the wavelength of the initial disturbance. We further assume that the initial fiber position is given by

$$\mathbf{X}(s,0) = (s, 0.05L \cdot \sin(2\pi s/L)).$$

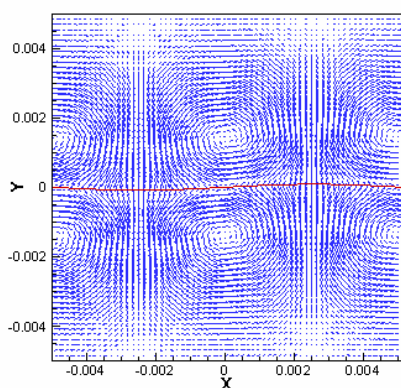
We carry out the computation using the immersed boundary method by taking  $L = 1 \text{ cm}$  and a time step size  $\Delta t = 10^{-5} \text{ s}$ . In Fig. 6, we have plotted the velocity and pressure fields at various times. It can be seen that the fiber moves from its initial



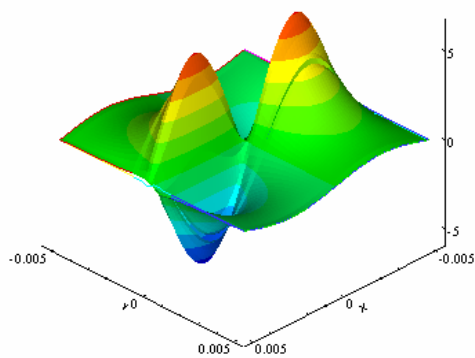
(a) velocity (t=0.017)



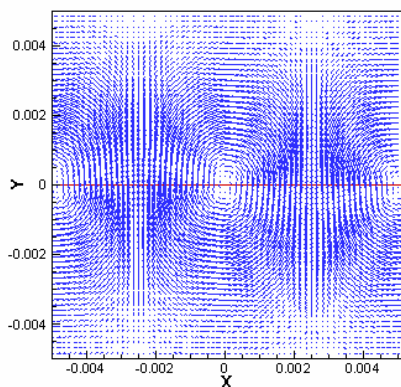
(b) pressure(t=0.017)



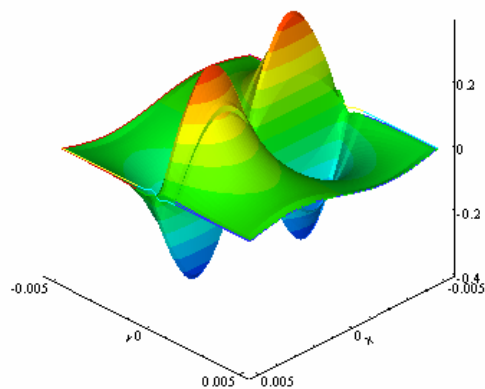
(c) velocity (t=0.034)



(d) pressure (t=0.034)



(e) velocity (t=0.085)



(f) pressure (t=0.085)

Figure 6: Plots for velocity and pressure field at three different times ( $\phi_n = 10 \text{ g} \cdot \text{cm}^2/\text{s}$ ).

position towards its equilibrium state, as predicted by the linear stability analysis. The fiber first reaches its equilibrium and continues its movement in the same direction until  $t=0.017$ , and then it starts to move in the opposite direction and its velocity

becomes zero again at time  $t=0.034$ . Because of viscous dissipation (non-zero real part of the eigenvalues), the fiber continues to oscillate while its amplitude decays until it finally reaches its equilibrium position asymptotically. Fig. 7 shows the comparison between the numerical and analytical results. It gives the maximum displacement of the fiber under two different bending modulus. The solid line is the analytical results, the dashed line is the numerical results and the straight line is the equilibrium position. We can see that the two decaying periods agree well, but the numerical results decay faster than the analytical ones, which becomes more obvious as the bending modulus increases.

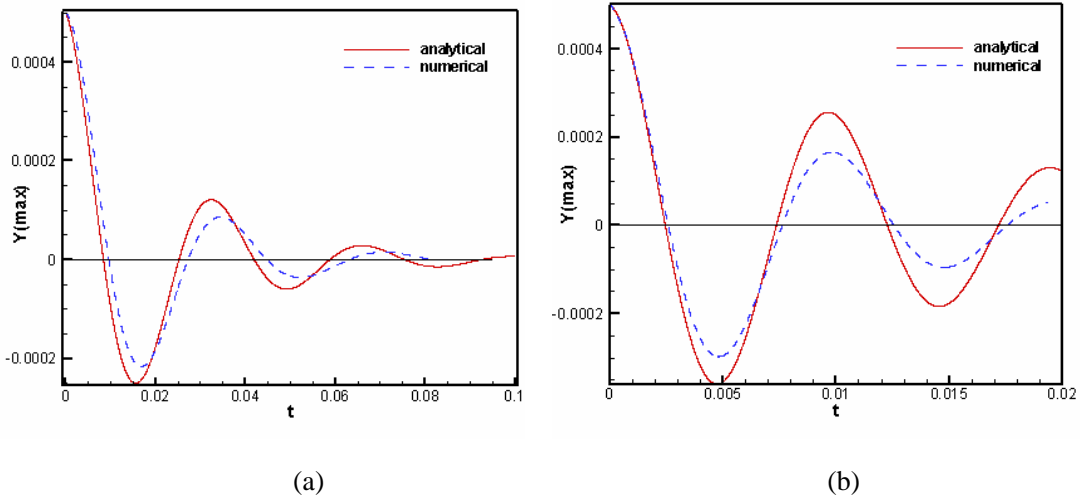


Figure 7: Comparison of the maximum displacement between the numerical and analytical results under two different bending modulus (a):  $\phi_n = 10 \text{ g} \cdot \text{cm}^2/\text{s}$  and (b):  $\phi_n = 10 \text{ g} \cdot \text{cm}^2/\text{s}$ .

### 3.4 Stiffness analyses

In [14], it is shown that the elastic fiber-fluid system (and consequently the immersed boundary method) is stiff due to the wide spread of decaying rates for low and high frequency modes. As the bending resistance is proportionally to the 5<sup>th</sup> power of the wave number, instead of the 3<sup>rd</sup> power for the in-plane tension, the difference between the decaying rates is much bigger, indicating that the problem for the coupled bending resistant membrane-fluid system is much more stiff. In this section we compare the stiffness of the sharp interface problem and the smoothed problem, which is more relevant to the immersed boundary method from the

computational point of view.

The variation in the magnitude of  $\text{Re}(\lambda^*)$  indicates the range of decay rates, and the larger the variation is, the wider the time scales are, vice versa. As seen in Fig.8, the difference in  $\text{Re}(\lambda^*)$  for smoothed problem is smaller than that for the sharp interface problem for the same range of wave numbers. This is because the high frequency modes are not captured by smoothed problem, due to the regularization of the Dirac Delta function.

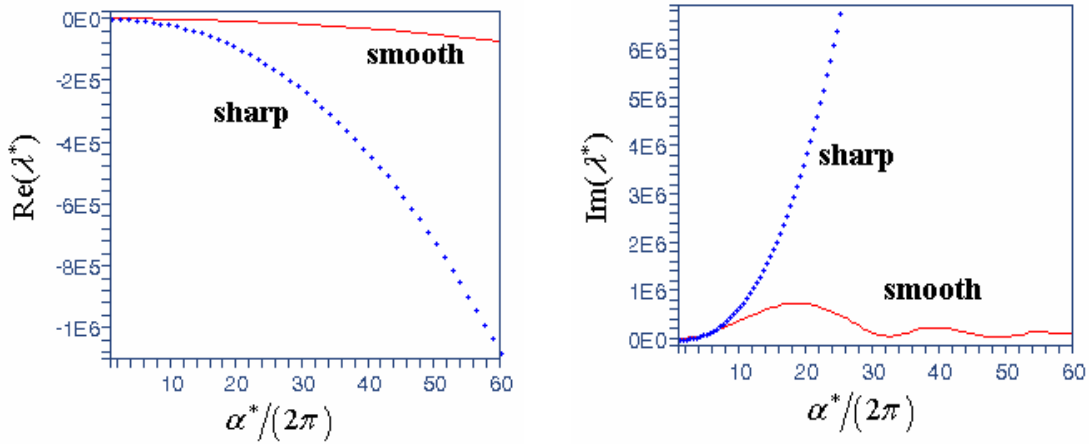


Figure 8: Comparison of  $\text{Re}(\lambda^*)$  and  $\text{Im}(\lambda^*)$  for the sharp interface and smoothed problem with parameters:  $Re = 1, Er = 10^3, \omega_n = 0$  and  $\varepsilon = 2/64$ .

The difference in  $\text{Im}(\lambda^*)$  for low and high frequency modes gives the frequency range of all oscillatory modes of the solution, and a large variation in  $\text{Im}(\lambda^*)$  points to modes with disparate frequencies. In Fig.8, it can be seen that for the sharp interface problem, the value of  $\text{Im}(\lambda^*)$  increases exponentially with wave number while for the smoothed problem the variation of  $\text{Im}(\lambda^*)$  is bounded. This is another indication that the smoothed problem is less stiff. Again, it can be attributed to the regularization alleviating the discontinuity in the physical variables between the two sides of the immersed boundary.

**Table I:** Comparison of the smallest decay rates and frequencies for the smallestwave number  $\alpha^* = 2\pi$  for various bending ratio ( $Re = 1$ )

Bending ratio	Smallest decay rate $Re(\lambda^*)$		Frequency $Im(\lambda^*)$	
	Sharp	Smooth	Sharp	Smooth
$1 - \omega_n$				
0.0	-80	-77	1039	1030
0.2	-139	-110	3159	3106
0.4	-159	-120	4360	4282
0.5	-167	-123	4853	4763
0.6	-174	-126	5301	5200
0.8	-186	-130	6102	5981
1.0	-196	-133	6811	6671

**Table II:** Comparison of the smallest decay rates and frequencies for the smallestwave number  $\alpha^* = 10\pi$  for various bending ratio ( $Re = 1$ )

Bending ratio	Smallest decay rate $Re(\lambda^*)$		Frequency $Im(\lambda^*)$	
	Sharp	Smooth	Sharp	Smooth
$1 - \omega_n$				
0.0	-1484	-980	11200	10022
0.2	-4896	-1085	170636	137015
0.4	-5773	-1086	242054	193539
0.5	-6089	-1086	270891	216332
0.6	-6361	-1086	296981	236943
0.8	-6816	-1086	343342	273544
1.0	-7193	-1086	384217	305795

In the following we present some numerical results for an immersed boundary with both elastic force and bending rigidity. Note that the normal elastic tension weight coefficient  $\omega_n$  varies from one to one:  $\omega_n$  equals zero when there is only elastic tension while  $\omega_n$  equals one when there is only bending tension. In Table I the results for the most dominant frequency  $\alpha^* = 2\pi$  with the slowest decay rate are given and in table II the results for  $\alpha^* = 10\pi$  are listed. It can be seen clearly that as bending ratio increases, the decay rate  $\text{Re}(\lambda^*)$  increases and the gap between the sharp interface and smoothed problems widens. It also has shown that bending tension affects the value of  $\lambda^*$  more, which indicates that the effects of regularization become significant when the bending effects become prominent. However, the difference between the  $\text{Im}(\lambda^*)$  values is relatively small for the two problems, suggesting that regularization has little effect once the oscillatory frequencies for the lowest frequency mode. Comparing table I and table II, it is concluded that bending effects is more important for higher frequency modes.

**Table III:** Comparison of maximum time step for bending and elastic force problems under various wavelengths (explicit scheme)

Wavelength	Maximum time step	
	Bending force ( $E_B=0.1$ )	Elastic force ( $C_{ES}=0.1$ )
0.01	1E-5	5E-4
1	0.1	5E-3
100	10	1E-4

In order to tesity above point more concretely, we give the comparison of maximum time step for bending and elastic force problems under various wavelengths in table III. All the results are obtained using the explicit immersed boundary method.

It is shown that for the larger wavelength (low frequency), the in-line elasticity is more restrictive while for the smaller wavelength (high frequency), the bending is more restrictive. We can conclude that, for a fiber with both bending and elastic force, the choice of time step is dominant for the bending force part when the explicit time stepping scheme is used and the time step should be very restrictive.

#### 4. Conclusion

In this paper we study the linear stability of a coupled system consisting of a two-dimensional membrane with bending resistance immersed in an incompressible, viscous fluid. We show that the system is linearly stable when perturbed by a small deformation from the membrane's rest state. The stability analysis of the immersed boundary method, applied to this system is also carried out. Furthermore, we show that the problem is stiff and the immersed boundary method reduces the stiffness due to the regularization (smoothing) of the singular force term. Compared to the problem involving fibers with elastic tension [14], the system considered here is much more stiff. For membranes with both in-plane elastic tension and bending rigidity, the bending effect is dominant for high frequency modes while the in-plane tension is more important for the low frequency modes. The results suggest that the computations for the coupled membrane-fluid with bending resistance are more difficult than those for the coupled fiber-fluid with elastic tension, especially on a relative fine grid. Because of the larger decay rate and highly oscillatory nature of the high frequency mode, the explicit time stepping scheme may become unstable even though the underlying physical system is stable. Therefore, implicit time stepping scheme such as the one proposed in [15] is highly desirable for the membrane-fluid system with bending resistance.

**Acknowledgment:** The authors would like to express their gratitude to John Stockie for sharing his insights and helpful discussions and referees for constructive comments.

## Reference

- [1] C.S. Peskin, Numerical analysis of blood flow in the heart. *J. Comput. Phys.* 1977, 25: 220-252.
- [2] C.S. Peskin and D.M. McQueen, A three-dimensional computational method for blood flow in the heart 1. Immersed elastic fibers in a viscous incompressible fluid. *J. Comput. Phys.* 1989, 81: 372-405.
- [3] R. Dillion, L.J. Fauci, and D. Gaver, A microscale model of bacteria swimming, chemotaxis, and substrate transport. *J. Theor. Biol.* 1995, 177:325-340.
- [4] L.J. Fauci and A. McDonald, Sperm motility in the presence of boundaries. *B. Math. Biol.* 1995, 57:679-699.
- [5] L.J. Fauci and C.S. Peskin, A computational model of aquatic animal locomotion. *J. Comput. Phys.* 1988, 77: 85-108.
- [6] D. C. Bottino, Modeling viscoelastic networks and cell deformation in the context of the immersed boundary method. *J. Comput. Phys.* 1998, 147:86-113.
- [7] A. L. Fogelson , Continuum models of platelet aggregation: Formulation and mechanical properties. *SIAM J. Appl. Math.* 1992, 52:1089-1110.
- [8] L. J. Fauci and A. L. Fogelson, Truncated Newton's methods and the modeling of complex immersed elastic structures. *Comm. Pur. Appl. Math.* 1993, 46:787-818.
- [9] C. D. Eggleton and A. S. Popel, Large deformation of red blood cell ghosts in a simple shear flow. *Phys. Fluids* 1998, 10:1834-1845.
- [10] R. P. Beyer and R. J. Leveque, Analysis of a one-dimensional model for the immersed boundary method. *SIAM J. Num. Anal.* 1992, 29:332-364.
- [11] C. Tu and C.S. Peskin, Stability and instability in the computation of flows with moving immersed boundaries: A comparison of three methods. *SIAM. J. Sci. Stat. Comput.*, 1992, 13(6):1361-1376.
- [12] J. M. Stockie, Analysis and computation of immersed boundaries, with application to pulp fibers. Ph.D. thesis, Institute of Applied Mathematics, University of British Columbia, 1997.
- [13] J. M. Stockie and B. R. Wetton, Analysis of stiffness in the immersed boundary method and implications for time-stepping schemes. *J. Comput. Phys.* 1999, 154: 41-64.
- [14] J. M. Stockie and B. R. Wetton, Stability analysis for the immersed fiber problem. *SIAM J. Appl. Math.* 1995, 55: 1577-1591.
- [15] R. J. LeVeque and Z. Li, The immersed Interface Methods for elliptic equations with discontinuous coefficients and singular sources. *SIAM J. Numer. Anal.* 1994, 31(4):1019-1044.
- [16] H. Huang and Z. Li, Convergence analysis of the immersed interface method. *IMA J. Numer. Anal.* 1999, 19:583-608.
- [17] H. Zhou and C. Pozrikidis, Deformation of liquid capsules with incompressible interfaces in simple shear flow. *J. Fluid Mech.* 1995, 283: 175-200.
- [18] C. Pozrikidis, The axisymmetric deformation of a red blood cell in uniaxial straining flow. *J. Fluid Mech.* 1990, 216: 231-254.
- [19] S. Osher and R. P. Fedkiw. Level set methods: an overview and some recent results. *J. Comput. Phys.* 2001, 169(2):463-502.
- [20] S. Osher and R. P. Fedkiw. Level Set Methods and Dynamic Implicit Surfaces. Springer-Verlag, New York, 2002.
- [21] C. Pozrikidis, Introduction to theoretical and computational fluid dynamics. New York:

Oxford University Press Inc,1999.

[22] C.S. Peskin, The immersed boundary method. *Acta Numerica* 2002, 11:1-39.

[23] E.A. Evans and R. Skalak, *Mechanics and Thermodynamics of Biomembranes*. CRC Press, Boca Raton,1980.

[24] C. Pozrikidis, *Modeling and simulation of capsules and biological cells*. CRC Press UK,2003.